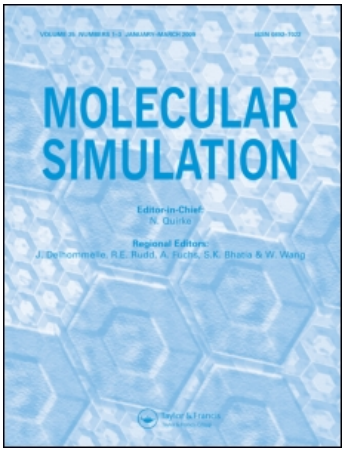

Molecular Simulation
Publication details, including instructions for authors and subscription information:
http://www.informaworld.com/smpp/title~content=t713644482

Effect of pore constriction on adsorption behaviour in nanoporous carbon slit pore: a computer simulation

A. Wongkoblap[a]; D. D. Do[a]
[a] Department of Chemical Engineering, University of Queensland, St Lucia, QLD, Australia

To cite this Article Wongkoblap, A. and Do, D. D.(2006) 'Effect of pore constriction on adsorption behaviour in nanoporous carbon slit pore: a computer simulation', Molecular Simulation, 32: 7, 539 — 549
To link to this Article: DOI: 10.1080/08927020600623657
URL: http://dx.doi.org/10.1080/08927020600623657

Molecular Simulation, Vol. 32, No. 7, 15 June 2006, 539–549

Taylor & Francis
Taylor & Francis Group

Effect of pore constriction on adsorption behaviour in nanoporous carbon slit pore: a computer simulation

A. WONGKOBLAP and D. D. DO*

Department of Chemical Engineering, University of Queensland, St Lucia, QLD 4072, Australia

(Received November 2005; in final form February 2006)

A Grand Canonical Monte Carlo simulation (GCMC) method is used to study the effects of pore constriction on the adsorption of argon at 87.3 K in carbon slit pores of infinite and finite lengths. It is shown that the pore constriction affects the pattern of adsorption isotherm. First, the isotherm of the composite pore is greater than that of the uniform pore having the same width as the larger cavity of the composite pore. Secondly, the hysteresis loop of the composite pore is smaller than and falls between those of uniform pores. Two types of hysteresis loops have been observed, irrespective of the absence or presence of constriction and their presence depend on pore width. One hysteresis loop is associated with the compression of adsorbed particles and this phenomenon occurs after pore has been filled with particles. The second hysteresis loop is the classical condensation–evaporation loop. The hysteresis loop of a composite pore depends on the sizes of the larger cavity and the constriction. Generally, it is found that the pore blocking effect is not manifested in composite slit pores, and this result does not support the traditional inkbottle pore hypothesis.

Keywords: Adsorption; Carbon slit pore; Finite-length pore; GCMC; Hysteresis; Pore constriction

1. Introduction

The computer simulation study of adsorption/desorption hysteresis loop is mainly carried out for mesoporous materials [1–4], and the pore blocking has been used as one of the reasons to explain the hysteresis between adsorption and desorption in gas adsorption. Two mechanisms for hysteresis have been put forward in the literature. One is the intrinsic property of the phase transition in a single idealized pore, while the other is associated with the interconnectivity of a pore network [1]. The adsorption isotherms on uniform mesoporous materials show a distinctly sharp and vertical pore filling, while experimental hysteresis loops of porous materials show either quasiparallel adsorption/desorption branches or a steeper desorption branch compared to the adsorption branch [2]. The former generally occurs for activated carbons [5]. To understand the mechanism of adsorption and desorption in activated carbon, computer simulations have been used to investigate the role of solid models in adsorption behaviour. To model porous carbon, they are typically assumed to compose of pores of different widths. For the simplicity of modelling, pores are assumed either infinite slit pores [6–8] or infinite cylindrical pores [9]. In reality, pores are neither infinite nor uniform. The infinite pore model is too ideal to reflect the activated carbon structure whose length is finite in lateral directions, rather than infinite [10], and it contains functional groups, chemical impurities and morphological defects on the basal graphene layers [11]. Real carbons have pores of different sizes and shapes, and they are interconnected at various points which strongly influence the adsorption behaviour [8].

Two molecular simulation methods, a molecular dynamics (MD) and a Monte Carlo simulation (MC), are being increasingly applied to solve numerous adsorption problems. The study of methane adsorption in slit pore with different interconnected porous structures using the MD method [3] and the study of argon adsorption in cylindrical pore having a constriction using the MC method [2,4] have been carried out to investigate the effect of the pore morphology on adsorption/desorption isotherms and hysteresis. To reveal the effects of pore length on the behaviour of adsorption

*Corresponding author. Tel.: +61-7-3365-4154. Fax: +61-7-3365-2789. E-mail: duongd@cheque.uq.edu.au

Molecular Simulation
ISSN 0892-7022 print/ISSN 1029-0435 online © 2006 Taylor & Francis
http://www.tandf.co.uk/journals
DOI: 10.1080/08927020600623657

isotherm, we have recently presented computer generated isotherms of argon in finite-length carbon slit pores whose two walls composed of three graphene layers with carbon atoms arranged in a hexagonal pattern [12]. The adsorption isotherms of argon in finite-length slit pores whose walls are a face centered cubic lattice structure [13–14], and those in finite-length cylindrical pores [2,9] have been presented in the literature to investigate the effects of pore length. The molecular simulations of gas adsorption in defective slit pores models or structural models of porous carbons have shown that the complex morphology of real porous carbons strongly influences the adsorption isotherm [15–20]. To obtain a reliable solid model that enables us to predict the behaviour of gas adsorption on activated carbon is still a challenging issue. Therefore, the aim of this work is to use a composite slit pore model that consists of two regions to study the effect of pore constriction on the adsorption behaviour in activated carbon. One region is the constricted region and the other is called the larger cavity region.

In this paper, the adsorption isotherms of argon in three simple pore models with constriction are obtained by using a Grand Canonical Monte Carlo simulation (GCMC). The differences among these models are the location of the constricted region. Detailed description of these models will be given in Section 2.2. We particularly study the effects of pore constriction on the adsorption behaviour in the case of constricted regions having widths between 6.5 and 16 A (2–4 times the fluid collision diameter). Computer generated adsorption isotherms of these models will be compared with those for either infinite or finite-length slit pores with uniform pore width.

2. Methodology

2.1 Fluid model

In this paper, argon is used as a model for Lennard-Jones fluids. The LJ parameters, $\sigma_{ff} = 3.405$ A and $\varepsilon_{ff}/k = 119.8$ K [6] and a cut-off radius in the calculation of energy of interaction of five times the collision diameter ($5\sigma_{ff}$) are used in this study. The potential energy of interaction between two particles is calculated using the Lennard-Jones 12–6 equation [6].

2.2 Solid model

The solid model used in this study is the carbon-based adsorbents whose pores typically have a slit-shaped geometry [12]. A simple slit pore of finite-length is modelled as a parallel pair of finite-length walls which consist of graphene layers and are perpendicular to the *Z*-axis. Each wall consists of graphene layers, and the interlayer spacing (Δ) between two adjacent layers is 3.354 A. The width *H* of this slit pore model is defined as the distance between a plane passing through all carbon atom centres of the outmost layer of one wall and the corresponding plane of the other wall. The configuration of carbon atoms in each layer takes the form of condensation of aromatic rings of six carbon atoms. The adjacent carbon–carbon distance is 1.42 A [11].

The LJ parameters for sp^2 carbon atom of the graphene layer, σ_{ss} and ε_{ss}/k, are 3.4 A and 28 K, respectively, [6]. The interaction energy between an argon particle and the carbon surface is calculated by summing the pairwise Lennard-Jones 12–6 equation between the argon particle and a carbon atom in the surface for the case of finite-length slit pores of uniform width. In the case of infinite pore of uniform width we use the Steele 10–4–3 potential. In the case of composite pore of either finite or infinite length the interaction energy is calculated by summing the pairwise Lennard-Jones 12–6 equation between an argon particle and a carbon atom of the pore walls. The cross molecular parameters are calculated from the Lorentz–Berthelot rule [6,12].

In this study, three different models of composite pore are used. The composite pore composes of two regions. The larger region is termed the larger cavity while the narrow one is termed the constricted region or simply the constriction. The first model assumes that the constriction is located at the centre of the solid model. Figure 1(a) shows the solid configuration for this model (for clarity we do not show all graphene layers). The second model assumes that the larger cavity is located at the pore centre (figure 1(b)). This model is similar to the inkbottle pore

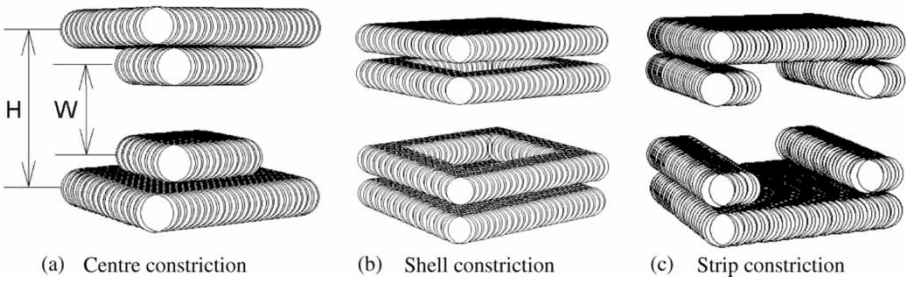

Figure 1. The solid configuration for the first (a), second (b), and third (c) models.

[3,21]. In the last model we assume that the larger cavity is connected between the two strips of constricted region (figure 1(c)). Hereafter, we will use the words centre, shell and strip constrictions to describe the first, second and third models, respectively.

2.3 Simulation method

For a finite pore model, all graphene layers are assumed to be square in size and the length of the pore has a linear dimension of 60 A ($17.62\sigma_{ff}$) in the x and y directions because it is reported in the literature [10] that the size of the graphene layer in activated carbon is between 20 and 70 A. We assume that the composite pore contains about 20% of the constriction volume, therefore we choose the length of constricted region of $8.8\sigma_{ff}$ in the x and y directions for the centre constriction. While the length of the constriction and that of the larger cavity in the x direction are $2.58\sigma_{ff}$ and $12.46\sigma_{ff}$, respectively, for the strip constriction. Unlike the centre constriction, the composite pore of shell constriction contains about 40% of the constriction volume. This is because we impose a constraint that the length of the constricted region should not be smaller than $2\sigma_{ff}$, therefore, the length of the larger cavity of $12.46\sigma_{ff}$ in the x and y directions (the length of the constricted region is $2.58\sigma_{ff}$ in one direction) are chosen. The top and bottom of the simulation box are two walls of the slit pore, and each wall consists of three and four graphene layers for the larger cavity and the constricted region, respectively. In the case of an infinite pore of either in the absence or presence of pore constrictions, a linear dimension of 60 A ($17.62\sigma_{ff}$) in the x and y directions is used and the lengths of $4.4\sigma_{ff}$ and $8.82\sigma_{ff}$ are taken for the constricted region and the larger cavity, respectively.

The widths for the constriction and the larger cavity regions of a composite pore are denoted as W and H, respectively. For a given value of H, the width of the constriction is calculated from the following equation.

$$W = H - n\Delta \tag{1}$$

where n is the number of graphene layers. In this work, we choose the composite pores listed in table 1 in our investigation.

For comparison, the simulations of argon adsorption in either finite or infinite slit pores with uniform pore widths W and H are also carried out. Hereafter, we will use the term shell-6/20 to refer to a composite pore having widths 6.5 and 20 A for the constriction and larger cavity, respectively, and the constriction has the shell configuration.

GCMC with the Metropolis algorithm [22,23] is used to obtain adsorption isotherm of argon in a slit pore. One GCMC cycle consists of one thousand displacement moves and attempts of either insertion or deletion with equal probability. For an adsorption branch of the isotherm, 10,000 GCMC cycles are typically needed for the system to reach equilibrium, and additional 10,000 cycles are used to obtain ensemble averages. For each point on the adsorption branch, we use an empty box as the initial configuration, and the simulation is carried out until the number of particles in the box does not change (in statistical sense). On the other hand, desorption branch of the isotherm is started with the chemical potential at the saturation condition ($P = P_0$), then the chemical potential is decreased to a new value. The equilibrium configuration of the previous chemical potential is used as the starting point for the new chemical potential, and the process is repeated until the simulation box is empty. For desorption branch of the isotherm, the number of GCMC cycle in the equilibration step is 10,000 cycles while in the sampling step 20,000 cycles are used to average the amount adsorbed. The cut-off radius of five times the collision diameter of fluid is fixed and used in the simulation. The displacement step length is initially chosen as 0.5 times the collision diameter of fluid, and it is decreased 5% when the acceptance ratio is <0.5 and increased 5% when this ratio is >0.5. All calculations are carried out at the boiling temperature of argon, 87.3 K. In the case of infinite pore, periodic boundary conditions are applied in x and y directions [22,23]. While in the case of finite pore, the particle move is rejected if the particle is attempted to be displaced to a position outside the simulation box.

Table I. The composite pores used in this investigation.

Composite pore	*W (A)*	*H (A)*
6/9	6.5	9
6/20	6.5	20
8/15	8	15
9/16	9	16
15/22	15	21.7
16/22	16	22.4

3. Results and discussions

We start our discussion by presenting the adsorption isotherms for infinite pores in the presence or absence of pore constrictions. Four composite pores with shell constriction, 6/9, 6/20, 9/16 and 16/22, are selected to study the adsorption behaviour and hysteresis loop. Next the adsorption isotherms obtained for infinite 9/16 composite pores having centre and strip constrictions will be compared with that obtained for the shell constriction, in order to study the effects of the pore constriction and the location of constriction on the adsorption behaviour. The effects of pore length are also studied and we use the centre-8/15 composite pore in this investigation. Finally, the discussion of the adsorption behaviour of finite-length pores with constriction will be presented.

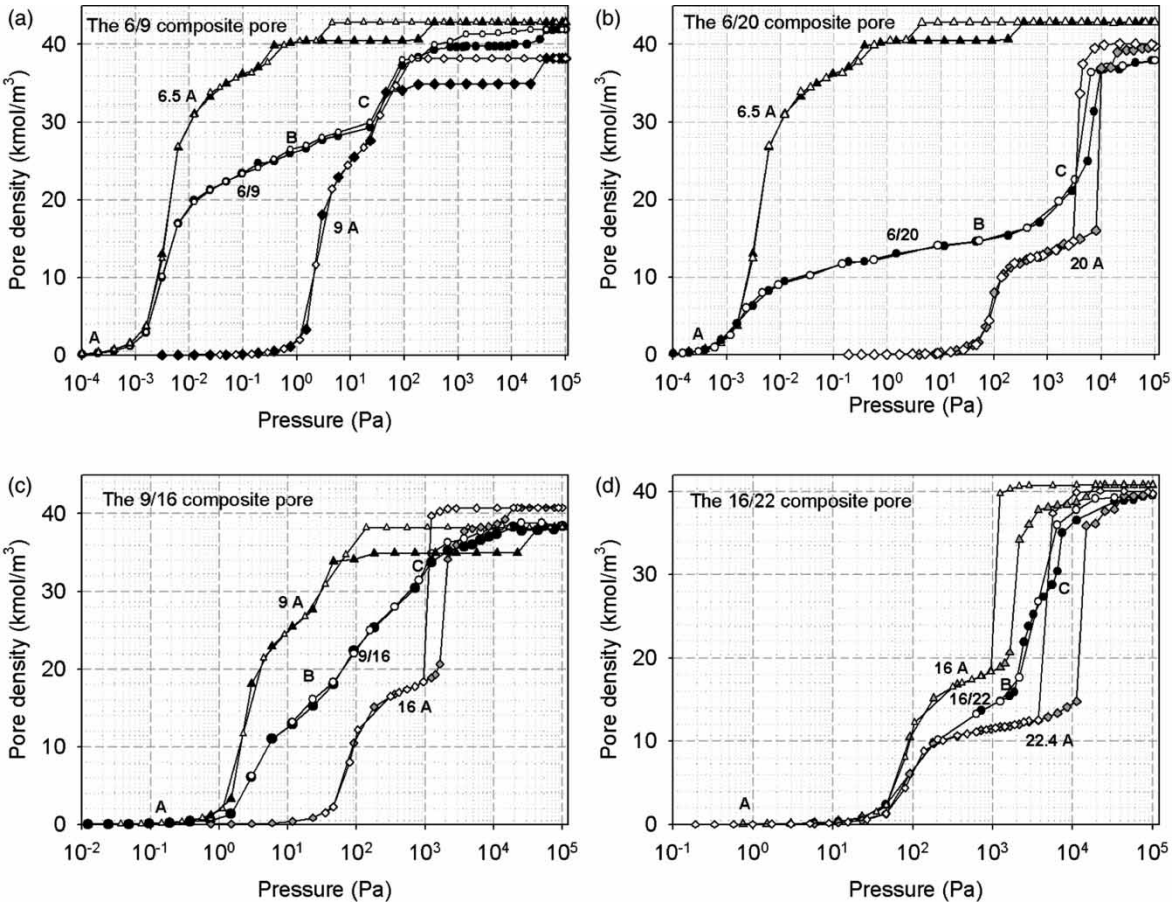

Figure 2. Adsorption isotherms of argon at temperature 87.3 K obtained for the composite pore, *W*/*H* (circle symbols; filled symbols for adsorption and unfilled symbols for desorption), that obtained for a uniform width of *W* (triangle symbols) and that obtained for a uniform width of *H* (diamond symbols).

3.1 Adsorption mechanism in infinite composite pore

The simulated isotherms versus pressure in semi-log scale for the shell-6/9, 6/20, 9/16 and 16/22 composite pores are shown in figure 2. The curve for the composite pore is the one with circle symbols (middle curve), while those for pores with uniform width of *W* and *H* are presented as curves with triangle and diamond symbols (top and bottom curves), respectively. For the shell-6/9, 6/20 and 9/16 composite pores, adsorption starts at the neck surrounding the interior larger cavity, and subsequently a shell of adsorbate particles surrounds the centre of the pore (this occurs in the range AB in figures 2(a),(b),(c)), and when the pressure is greater than that at B, adsorption continues to occur in the larger cavity until it is filled. The behaviour of the shell-16/22 composite pore (figure 2(d)) is different from those of the three smaller composite pores. We observe that the adsorbed phase is started by forming the two contact layers adjacent to the two walls at low pressures and this occurs at both the constriction and the larger cavity (the range AB in figure 2(d)). When the pressure increases further, these contact layers are completed and eventually the whole composite pore is filled, starting in the constricted region (this is the range BC in figure 2(d)) and then the larger cavity. The point C of figure 2(d) corresponds to the pressure of 5600 Pa in figure 3(a), at which the constricted region is completely filled and the inner core of the larger cavity still contains two contact adsorbed layers.

We have observed in figure 2 two types of hysteresis loop in micropores of uniform width; one is occurred in pores having width smaller than 9 A. The change in density is continuous because of the continuous filling of a single layer in 6.5 A pore and nearly two perfect layers in 9 A pore. Upon the completion of the filling process the adsorption isotherm exhibits a small jump in density at the compression pressure, at which the molecular arrangement allows further small addition of molecules into the pore. This compression leads to an average density which is close to the solid density for pore width of 6.5 A and a density of a highly compressed liquid at pressure close to the vapour pressure for pore width of 9 A. Along the desorption branch, the pressure has to be reduced below the compression pressure before the adsorbed phase is changed from a "solid" state or "highly compressed" state to a liquid state. This hysteresis loop is called the compression loop. Another hysteresis loop is observed in pores having width >9 A, typical of mesopore where a sharp change in density is observed in both adsorption and

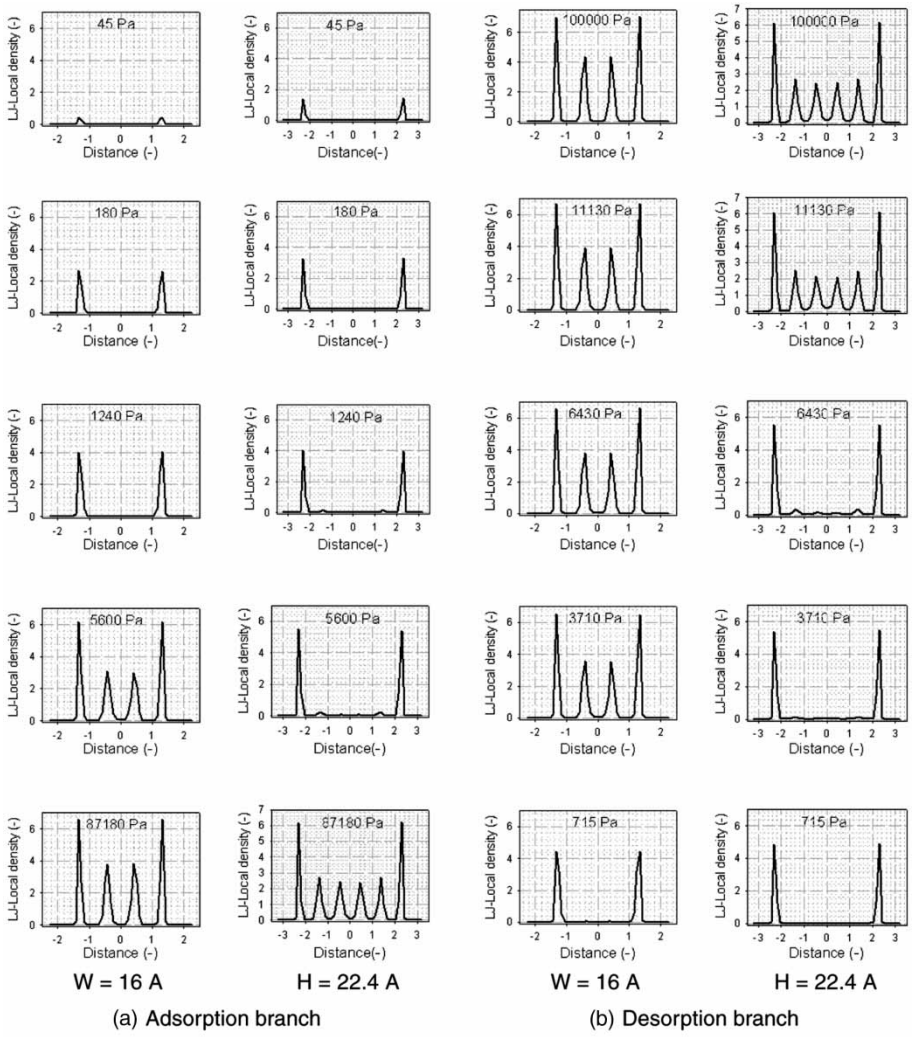

Figure 3. Local density distributions versus distance from pore wall with various values of pressure for the constriction (16 A) and the larger cavity (22.4 A) of the shell-16/22 composite pore.

desorption branches. This loop is called the condensation–evaporation loop.

Four types of hysteresis loop are specified as H1, H2, H3 and H4 by the IUPAC classification of adsorption isotherms [24]. Types H1 and H4 are characterized as the "extreme types" where branches are "almost vertical (H1) and nearly parallel (H4) over an appreciable range of gas uptake" [24] while the others are "intermediate between these two extremes" [13]. We have found that hysteresis loop for the shell-6/9 composite pore is a compression loop because its corresponding uniform pores of 6.5 and 9 A have compression loops. This loop is H4 type. In the case of larger shell-16/22 composite pore, the hysteresis loop is of the type of condensation–evaporation, and this is so because the corresponding pores of uniform width (16 and 22.4 A) exhibit this type. The only subtle difference is that the hysteresis loop of the composite pore is of H3 type. Thus it can be concluded that if the individual pores of uniform width exhibit hysteresis loop of one type (i.e. either compression loop or condensation–evaporation loop), the hysteresis loop of the composite pore will be of the same type. In the case of condensation–evaporation type, the hysteresis loop of the composite pore is slant (H3 type), which is different from the vertical behaviour of the individual pores. However, in the case where individual pores of uniform width exhibit different types of hysteresis loop, the hysteresis loop of the composite pore can be of either type. This depends on the width of the larger cavity. The shell-6/20 composite pore gives the condensation–evaporation loop, while the shell-9/16 composite pore exhibits the compression loop of H2 type. The pattern of hysteresis loop for a composite pore is either an asymmetrical loop of type H2 or H3, or a symmetrical loop of type H1 or H4. This depends on relative widths of the constriction and the larger cavity. It should be noted that the hysteresis loop of individual pore of uniform width is either type H1 or H4.

In figure 3(a), we show the local density distribution versus distance from the pore wall for the shell-16/22 composite pore along the adsorption branch for five values of pressure (45, 180, 1240, 5600 and 87,180 Pa). For clarity, we present the local density distribution of each

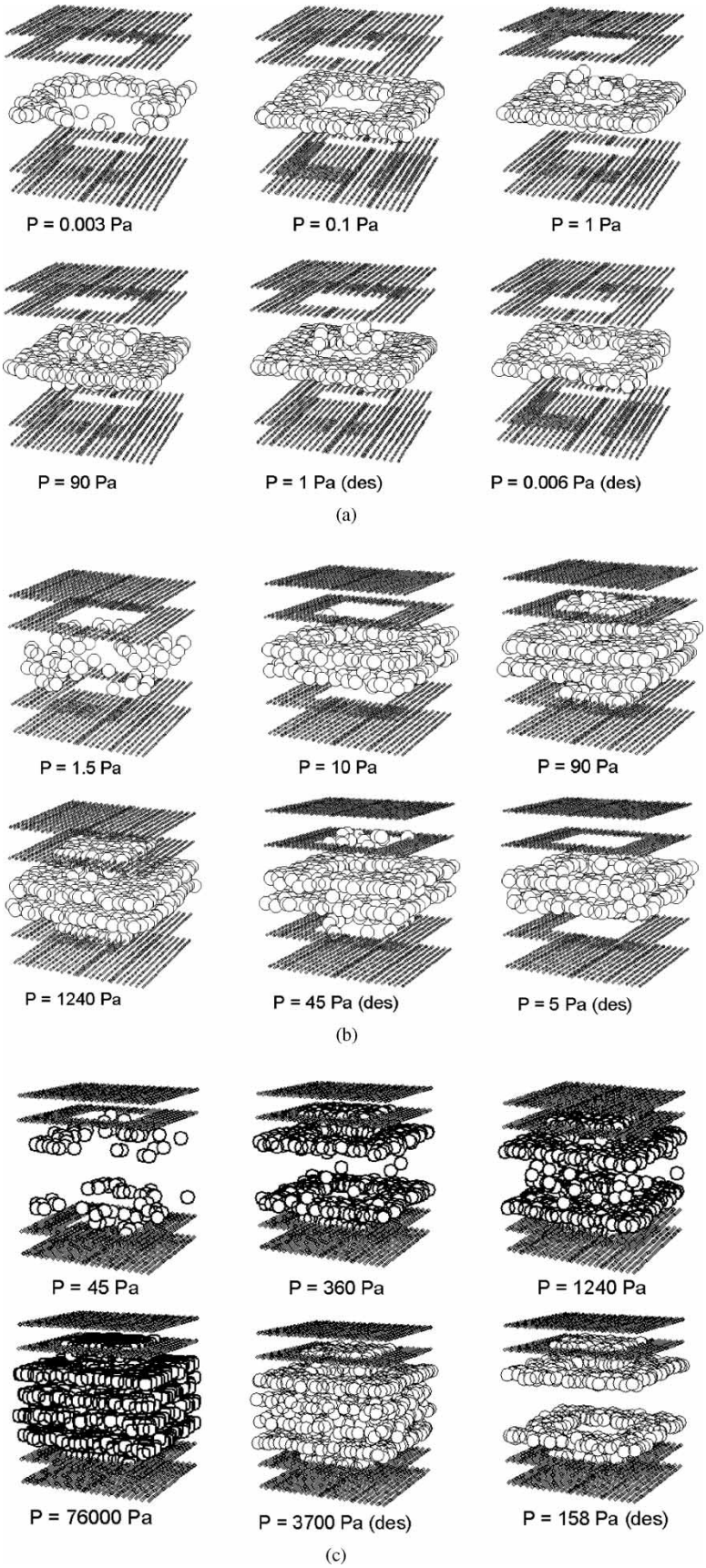

Figure 4. (a) Snapshot of argon particles in infinite slit pore for the shell-6/9 composite pore; (b) snapshot of argon particles in infinite slit pore for the shell-9/16 composite pore; (c) snapshot of argon particles in infinite slit pore for the shell-16/22 composite pore.

region separately rather than clustering them in one figure. As clearly seen in this figure, the numbers of layers in the 16 and 22.4 A segments of the composite pore are four and six, respectively. At low pressures, we observe the formation of two adsorbed layers for both the constricted region and the larger cavity (45, 180 and 1240 Pa, and these cover the range AB in figure 2(d)). At 5600 Pa, the constricted region is filled with adsorbate molecules, resulting in further two layers in the inner core, while the larger cavity remains with two contact layers (this is point C in figure 2(d)). When the pressure is further increased, the composite pore is completely filled with four and six layers in the constriction and the larger cavity, respectively.

The local density distribution for the desorption branch is shown in figure 3(b). At the saturated vapour pressure (100,000 Pa) the composite pore is completely filled with adsorbate, and this remains so until the pressure is 6430 Pa, at which we observe the evaporation of the inner core of the larger cavity while the constricted region remains filled. This suggests that the evaporation of the larger cavity is not inhibited by the pore blocking of the constriction. Our simulation study of the desorption mechanism in infinite composite pores gives the similar behaviour as observed by Sarkisov and Monson [3], and this phenomenon is a cavitation effect which has been presented in the literature [2–3,25]. This evaporation becomes completed at 3710 Pa. At even lower pressure (715 Pa), we observe the complete evaporation of the inner core of the constricted region and both regions now only have two contact layers remaining. Any further reduction in pressure from 715 Pa will result in the decrease of the concentrations of all contact layers.

In figure 4 we show snapshots of adsorption and desorption in the infinite composite pores at various values of pressure. In this figure, black spheres represent carbon atoms, while white spheres are argon particles. These snapshots show that the filling and emptying of the larger cavity are possible even when the constriction is completely occupied with adsorbate molecules. This means that the pore blocking effect is not observed in our investigation of the composite pore whose constricted region is of graphitic nature as the cavity.

3.2 Effects of the type of pore constriction on the adsorption isotherm

Next we study the effects of the constriction configuration on adsorption in infinite composite pores. The GCMC simulation results for the 9/16 composite pore are plotted in figure 5 for three different constriction configurations. For comparison we also present in the same figure the adsorption isotherms of infinite pores of uniform width of 9 and 16 A.

Due to the presence of pore constriction, the following features are observed for the adsorption isotherms of the composite pore: (i) a greater adsorbed amount at pressures lower than the pore filling point; (ii) a smaller hysteresis loop; and (iii) an attenuated jump of phase transition comparing with that of the pore of uniform width, whose value is the same as that of the larger cavity ($H = 16$ A) of the composite pore. The adsorption and desorption behaviours observed in the case of centre and strip constrictions are the same as those in the case of shell constriction in the sense that the adsorbed phase is started by forming two contact layers at the constricted region and then at the larger cavity. Once these layers have been completed, the inner core of the composite pore is filled. On desorption process, the emptying of the inner core is observed even though the constriction remains filled with the adsorbate molecule. Thus the topology of constriction does not alter the adsorption and desorption behaviours that we have observed in the last section with the shell configuration. We note that the difference of adsorbed amounts for these three models of pore constriction shown in figure 5(a) is due to the different pore volumes of the constricted region and the larger cavity. When the volume ratio of these two regions is kept the same, the adsorption

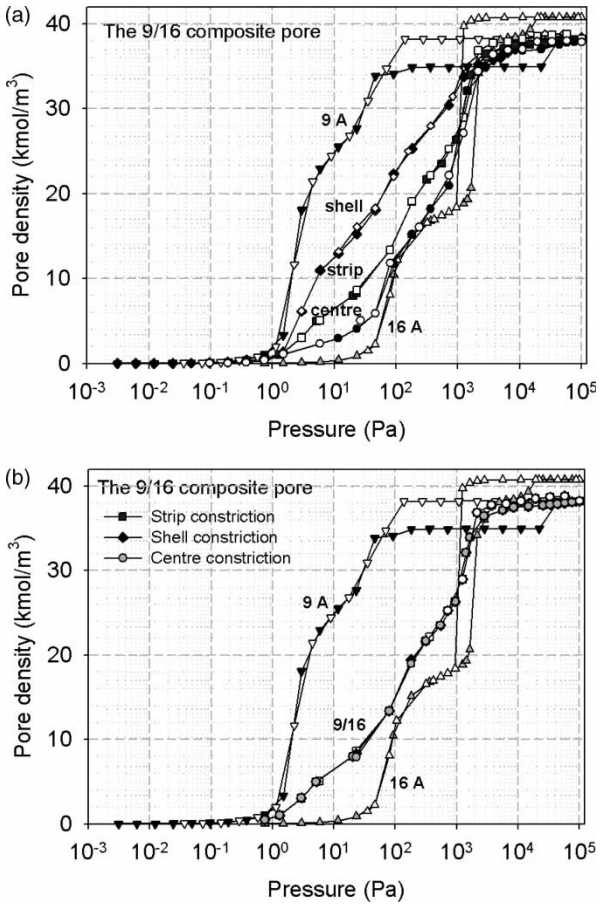

Figure 5. Adsorption isotherms of argon in infinite pore of the 9/16 composite pore at 87.3 K for the shell constriction (diamond symbols; filled symbols for adsorption and unfilled symbols for desorption), for the centre constriction (circle symbols), for the strip constriction (square symbols), for pore of 9 A width (downward triangular symbols), and for pore of 16 A width (upward triangle symbols): (a) for the different volume ratio; (b) for the same volume ratio of the constriction and the larger cavity.

isotherms are practically insensitive to the type of constriction as shown in figure 5(b).

3.3 Effects of pore length on the adsorption isotherm of composite pore

To study the effects of pore length, we compare the adsorption isotherms between a finite-length composite pore and an infinite composite pore. We use the centre-8/15 composite pore in this comparison. The simulated isotherms for these pores are shown in figure 6. The isotherm for finite composite pore is lower than that for infinite composite pore, and this is due to the lower solid–fluid potential in the region of pore mouth of the finite composite pore where argon particles interacts with lesser number of carbon atoms. Furthermore the isotherm of finite composite pore is smoother and shallower, and the hysteresis loop is either smaller or not observed. This is due to the presence of a meniscus, at which evaporation of argon particles from the adsorbed phase into the surrounding bulk fluid is readily facilitated.

Adsorption isotherms for three topologies of constriction for the 8/15 finite composite pore are shown in figure 7, and they are compared with behaviour of finite pores of uniform width of 8 and 15 A. The same behaviour is observed in the finite composite pores as that in the infinite composite pores dealt with earlier, that is the adsorption isotherms of these composite pores are greater than that of pore of uniform width of 15 A (the same width as the larger cavity of composite pore). This is due to the adsorption of argon particles in the constriction, which is narrower and possesses greater solid–fluid interaction potential.

We now study the adsorption isotherms and hysteresis loops of argon for the shell-8/15 and 15/22 finite composite pores. The percentage of pore volume contributed by the constricted region is 40%. The adsorption isotherms obtained for these composite pores are shown in figure 8. We observe again the lower adsorbed amounts, the smoother isotherms and the smaller hysteresis loops in

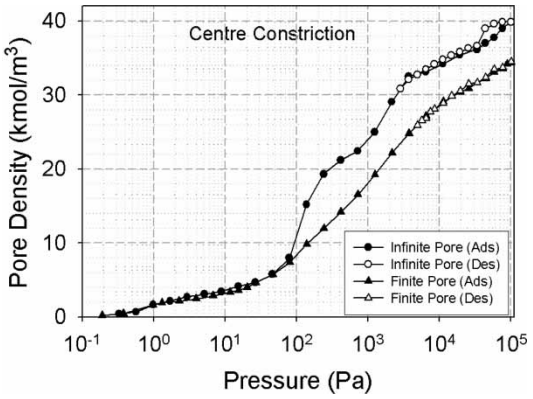

Figure 6. Adsorption isotherm of argon for the centre-8/15 composite pore of infinite length (circle symbols; filled symbols for adsorption and unfilled symbols for desorption) and that of finite-length (triangle symbols).

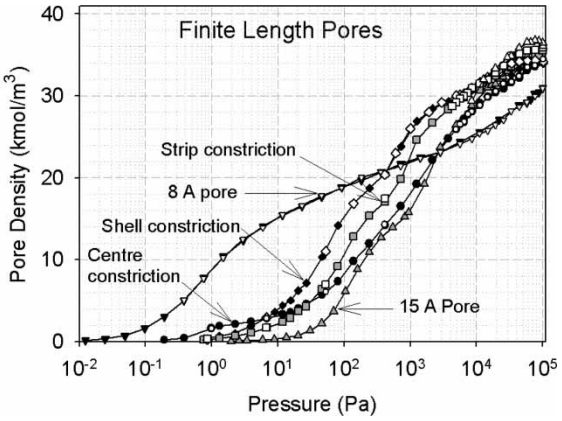

Figure 7. Adsorption isotherm of argon in finite pores at 87.3 K for the 8/15 composite pore of shell constriction (diamond symbols; filled symbols for adsorption and unfilled symbols for desorption), for that of centre constriction (circle symbols), for that of strip constriction (square symbols), for that of 8 A uniform width (downward triangle symbols), and for that of 15 A uniform width (upward triangle symbols).

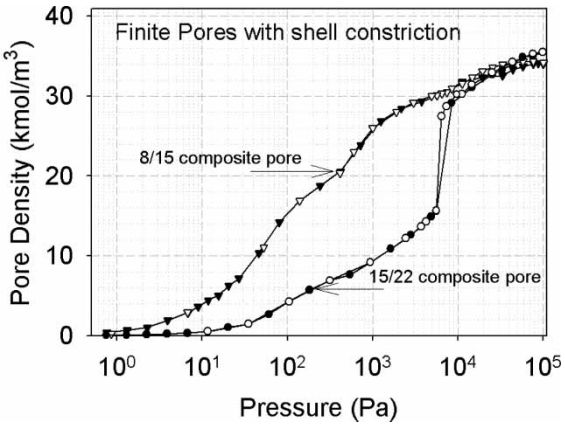

Figure 8. Adsorption isotherm of argon at 87.3 K for the shell-8/15 finite composite pore (triangle symbols; filled symbols for adsorption and unfilled symbols for desorption) and that for the shell-15/22 finite composite pore (circle symbols).

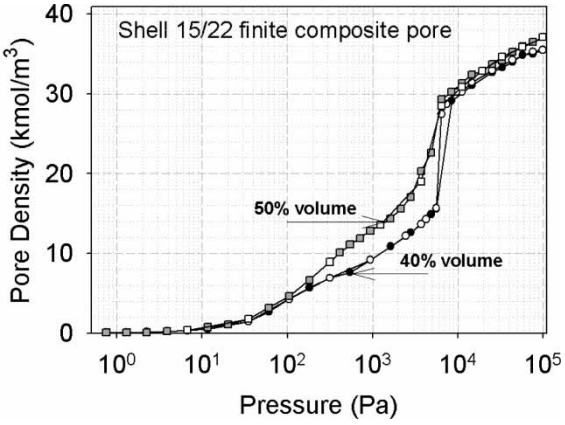

Figure 9. Adsorption isotherm of argon at 87.3 K for the shell-15/22 finite composite pore contained 50% of the constriction volume (square symbols; filled symbols for adsorption and unfilled symbols for desorption) and that for the shell-15/22 finite composite pore contained 40% of the constriction volume (circle symbols).

these finite composite pores comparing with those shown in figure 2 for infinite composite pores. This is due to the effects of pore length on the adsorption isotherms. We also observe that the pore filling point for the shell-15/22 finite composite pore is shifted to a lower pressure comparing to a finite pore of uniform width of 20 A [12] and this is due to the effect of the constriction on the adsorption.

In our investigation of adsorption of argon for infinite and finite composite pores, we observe that in desorption process the larger cavity can empty, although, the constricted region remains filled and this behaviour is the same as that observed for inkbottle geometry by Sarkisov and Monson [3]. However, these observations are in contrast with the general concept of pore blocking that the evaporation from the larger cavity cannot happen until the constriction has emptied. Let us further substantiate this by studying the effect of the constricted region length on the adsorption behaviour for finite composite pore to see whether the constriction could retard the desorption of the larger cavity. We chose two shell-15/22 composite finite pores; one contains 40% of the constriction volume while the other one is 50%. The adsorption isotherms for these two composite pores are shown in figure 9 and snapshots for these composite pores are shown in figure 10. While figure 11 shows the local density distributions for the constriction and the larger cavity of these composite pores along the adsorption branch. Four values of low pressure region in figure 11 are 20, 35, 105 and 180 Pa.

We have found that by increasing the constriction volume, the following significant features can be

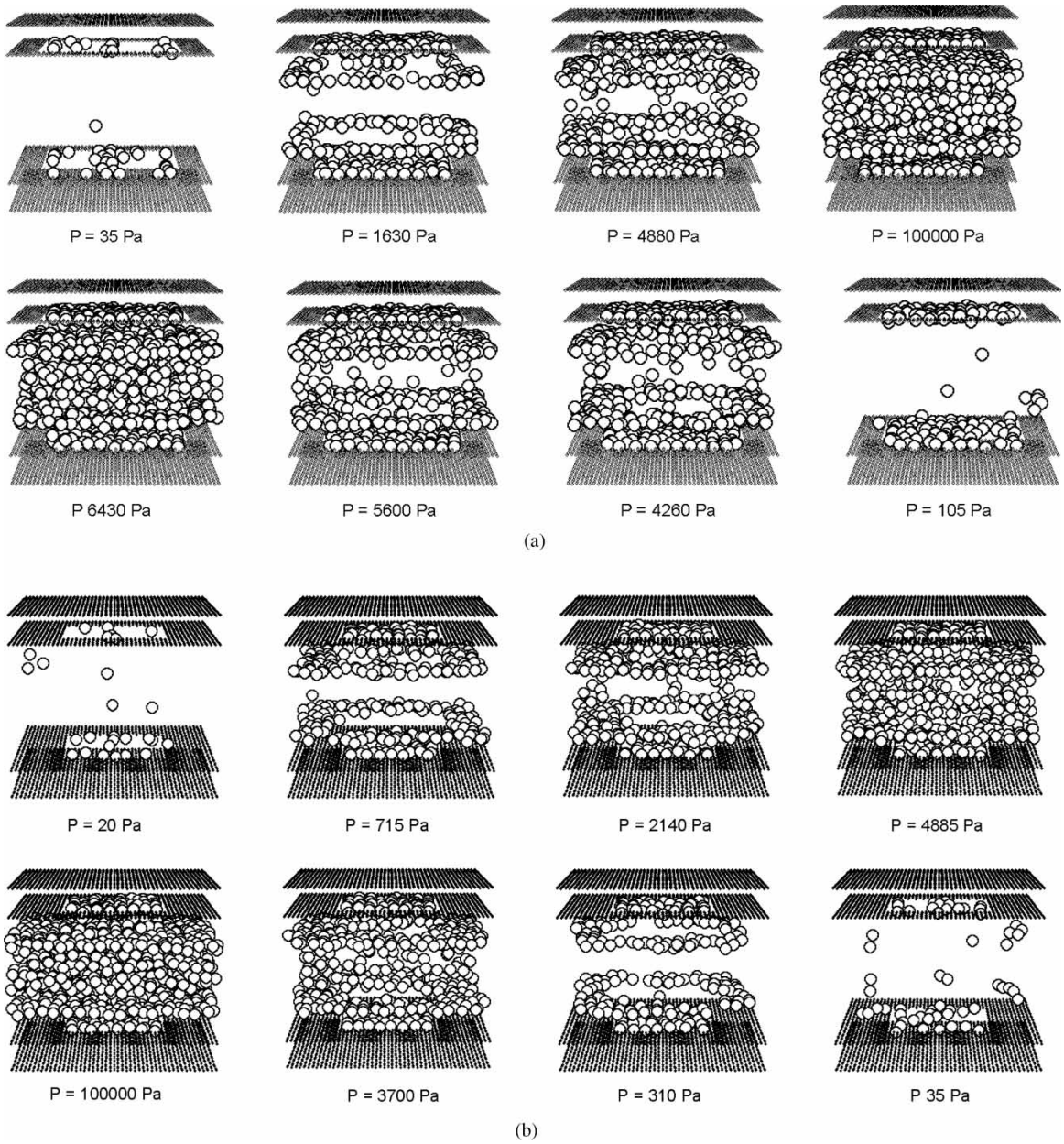

Figure 10. (a) Snapshots of argon particles in the shell-15/22 finite composite pore (40% of the constriction volume); (b) snapshots of argon particles in the shell-15/22 finite composite pore (50% of the constriction volume).

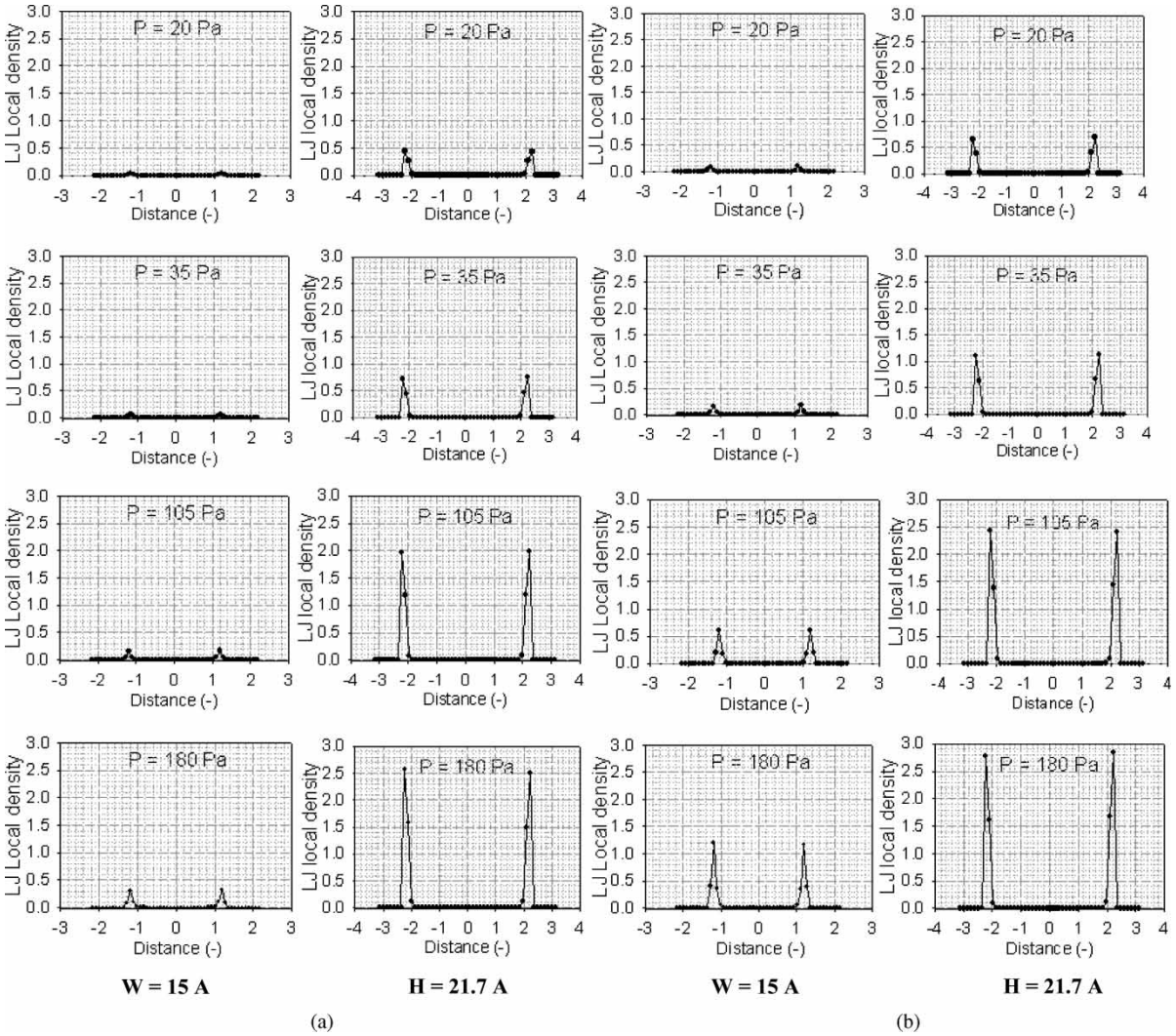

Figure 11. Local density distribution versus distance from pore wall with four values of low pressure for the shell-15/22 finite composite pores; (a) contained 40% of the constriction volume; (b) contained 50% of the constriction volume.

observed: (i) a smoother isotherm, and (ii) a greater adsorbed amount. The microscopic behaviour for these two composite pores shows few differences from each other at low pressures and so do the density distributions in figure 11. In the case of 40% constriction, the adsorbed phase starts by formation of two contact layers mostly in the larger cavity and smaller amount in the constricted region as one can observe in figure 10(a) at 35 Pa. This is substantiated in figure 11(a) where we show the local density distributions of the two regions. The formation of two contact layers in the larger cavity increases faster (the density increases from 0.5 to 2.5 in the pressure range from 20 to 180 Pa), while that in the constricted region only shows a small increase. This is due to the fact that argon particles in the cavity interact with more carbon atoms (those on the cavity walls as well as those at the inside edges of the graphene layers of the constriction) than those in the constriction. Since the constriction in this case is 15 A, there is no enhancement in the solid–fluid potential and therefore the formation of contact layers is faster in the cavity than in the constriction. This phenomenon is also observed in the case with 50% constriction, but the density of the contact layers in the constriction increases a bit faster than in the case of 40% because argon has greater number of carbon atoms to interact with (figures 10(b) and 11(b)).

When the pressure further increases and these contact layers are completed, the usual pattern of pore filling takes place. The pores are filled at the constriction and then the inner cores of the larger cavity. The reverse process is occurred in the desorption branch and the effect of pore blocking is not observed in the finite composite pore, which is the same conclusion that we have derived earlier with infinite composite pores. Therefore the constriction length does not affect the desorption behaviour for the composite pores.

4. Conclusions

In this paper, we have presented the adsorption of argon in carbon composite pores of finite and infinite lengths and

considered different topologies of pore constrictions using a GCMC simulation. Two types of hysteresis loop are observed. One is the compression loop which occurs in pores having width smaller than 9 A, and the other is the condensation–evaporation loop, observed in pores larger than 9 A. Both types of hysteresis loop can be found in the composite pore. The pore connectivity alters the pattern of adsorption–desorption hysteresis loop, compared to those of corresponding pores of uniform width.

The adsorption hysteresis in the case of finite composite pore is smaller and round when compared with that in the case of infinite composite pore, and these loops, in turn, are smaller than those of pores of uniform width. We have also presented the microscopic configurations and the adsorption isotherms for different solid models. It is shown that, the adsorbed phase is generally started by forming the initial two contact layers at the constriction then at the larger cavity and subsequently filling the inner cores. In desorption process, the behaviour is reverse and we cannot observe the pore blocking effect in both finite and infinite composite pores.

Acknowledgements

This project is supported by the Australian Research Council. We also acknowledge the Royal Thai Government for financial support in the form of scholarship to AW.

References

[1] P.C. Ball, R. Evans. Temperature dependence of gas adsorption on a mesoporous solid: capillary criticality and hysteresis. *Langmuir*, **5**, 714 (1989).

[2] B. Coasne, R.J.-M. Pellenq. A grand canonical Monte Carlo study of capillary condensation in mesoporous media: effect of the pore morphology and topology. *J. Chem. Phys.*, **121**(8), 3767 (2004).

[3] L. Sarkisov, P.A. Monson. Modeling of adsorption and desorption in pores of simple geometry using molecular dynamics. *Langmuir*, **17**, 7600 (2001).

[4] B. Coasne, R.J.-M. Pellenq. Grand canonical Monte Carlo simulation of argon adsorption at the surface of silica nanopores: effect of pore size, pore morphology and surface roughness. *J. Chem. Phys.*, **120**(6), 2913 (2004).

[5] J. Skalny, E.E. Bodor, S. Brunauer. Investigations of a complete pore-structure analysis of carbon adsorbents. *J. Colloid Interface Sci.*, **37**, 476 (1971).

[6] D.D. Do, H.D. Do. Refined method of potential enhancement in the equilibria characterization of activated carbon. Comparison with GCMC and DFT. *Langmuir*, **19**, 8302 (2003).

[7] C. Nguyen, D.D. Do. A new method for the characterization of porous materials. *Langmuir*, **15**, 3608 (1999).

[8] B. McEnaney, T.J. Mays, J. Rouquerol, F. Rodriguez-Reinoso, K.S.W. Sing, K.K. Unger. Characterisation of porous solids IV. In *Simulation Studies of Pore Blocking Phenomena in Model Porous Networks*, M. Maddox, N. Quirke, K.E. Gubbins (Eds.), The Royal Society of Chemistry, Cambridge (1997).

[9] M. Maddox, D. Ulberg, K.E. Gubbins. Molecular simulation of simple fluids and water in porous carbons. *Fluid Phase Equilibr.*, **104**, 145 (1995).

[10] R.E. Franklin. Crystallite growth in graphitizing and non-graphitizing carbons. *Proc. Roy. Soc.*, 209 (1951).

[11] D.D. Do. *Adsorption Analysis: Equilibria and Kinetics*, Imperial College Press, New Jersey (1998).

[12] A. Wongkoblap, S. Junpirom, D.D. Do. Adsorption of Lennard-Jones fluids in carbon slit pores of a finite length. A computer simulation study. *Adsorpt. Sci. Technol. J.*, **23**, 1 (2005).

[13] M.D. Donohue, G.L. Aranovich. Adsorption hysteresis in porous solids. *J. Colloid Interface Sci.*, **205**, 121 (1998).

[14] W.J. Stroud, J.E. Curry, J. Cushman. Capillary condensation and snap-off in nanoscale contacts. *Langmuir*, **17**, 688 (2001).

[15] J. Pikunic, C. Clinard, N. Cohaut, K.E. Gubbins, J.-M. Guet, R.J.-M. Pellenq, I. Rannou, J.-N. Rouzaud. Structural modeling of porous carbons: constrained reverse Monte Carlo method. *Langmuir*, **19**, 8565 (2003).

[16] B. Coasne, et al. *Material Research Society Proceeding*, pp. 790 (2003).

[17] M.J. Biggs, A. Buts, D. Williamson. Molecular simulation evidence for solidlike adsorbate in complex carbonaceous micropore structures. *Langmuir*, **20**, 5786 (2004).

[18] J. Pikunic, P. Llewellyn, R. Pellenq, K.E. Gubbins. Argon and nitrogen adsorption in disordered nanoporous carbons: simulation and experiment. *Langmuir*, **21**, 4431 (2005).

[19] A. Striolo, K.E. Gubbins, A.A. Chialvo, P.T. Cummings. The effect of pore connectivity on water adsorption isotherms in non-activated graphitic nanopores. *Adsorption*, **11**, 337 (2005).

[20] J.-C. Liu, P.A. Monson. Molecular modeling of adsorption in activated carbon: comparison of Monte Carlo simulations with experiment. *Adsorption*, **11**, 5 (2005).

[21] B. Libby, P.A. Monson. Adsorption/desorption hysteresis in inkbottle pores: a density functional theory and Monte Carlo simulation study. *Langmuir*, **20**, 4289 (2004).

[22] D. Frenkel, B. Smit. *Understanding Molecular Simulation*, Academic Press, New York (2002).

[23] R.J. Sadus. *Molecular Simulation of Fluids, Theory, Algorithms and Object-Orientation*, Elsevier Science B.V., Amsterdam (1999).

[24] P.I. Ravikovitch, A.V. Neimark. Experimental confirmation of different mechanisms of evaporation from ink-bottle type pores: equilibrium, pore blocking and cavitation. *Langmuir*, **18**, 9830 (2002).